Preparation of Layered MnO_2 via Thermal Decomposition of $KMnO_4$ and Its Electrochemical Characterizations

Sa Heum Kim, Sung Jin Kim,† and Seung M. Oh*

Division of Chemical Engineering and Institute of Chemical Process, College of Engineering, Seoul National University, Seoul 151-742, Korea, and Department of Chemistry, Ewha Womans University, Seoul 120-750, Korea

Received March 17, 1998. Revised Manuscript Received December 29, 1998

We report here the preparation of layered MnO_2 and the preliminary results on its cathodic performance in Li secondary batteries. The thermal decomposition of $KMnO_4$ powder at 250−1000 °C in air produces $K_xMnO_{2+\delta}\cdot yH_2O$ ($x = 0.27-0.31$, $\delta = 0.07-0.13$, and $y = 0.47-0.89$) with a product yield of 67−79% based on the Mn molar quantity. It can be judged from the Rietveld refinement on the X-ray diffraction pattern that the 800 °C-prepared sample has a layered structure (hexagonal unit cell, space group = $P6_3/mmc$, $a = 2.84$ Å, and $c = 14.16$ Å), where the K^+ ions and H_2O molecules reside at the interlayer trigonal prismatic sites (P2-type structure). Contrary to the previous findings whereby the layered MnO_2 transforms to α-/γ-MnO_2 phases or manganese suboxides at >450 °C, such impurities are negligible in this synthesis even at higher temperatures. The success of synthesis is ascribed to the high population of K^+ ions in the pyrolyzing media that act as pillaring cations to stabilize the layered framework. In addition, the absence of a suboxide transition is indebted to the highly oxidizing species such as O_2, MnO_4^{2-} and MnO_4^{3-}, which are produced during the pyrolyzing process. The materials show a powder density as high as 1.36 g cm^{-3} and the Mn^{4+} fraction of >85%, which gives a theoretical capacity of 210−230 mA h g^{-1} based on a one-electron charge/discharge reaction. A higher product yield up to >98% is achieved by pyrolyzing $KMnO_4$ with an addition of manganese suboxides (Mn_2O_3, Mn_3O_4, or MnO). Finally, the preliminary cell tests show that the materials give some promising features as the cathode materials for Li secondary batteries.

Introduction

The layered oxides Li_xNiO_2 and Li_xCoO_2 and spinel $Li_xMn_2O_4$ have been intensely studied for their applications to the cathode materials in Li secondary batteries.[1−4] Among those, Li_xCoO_2 has already been commercialized.[5] Li_xNiO_2 has several favorable features, such as the lower cost of nickel and higher capacity, but its synthesis is more difficult than the other oxides. The spinel $Li_xMn_2O_4$ presents an advantage over the layered ones because of the low cost of Mn and its easier preparation, but these advantages are largely offset by the lower rate capability, lower theoretical capacity, and higher cell voltage. The first disadvantage stems from its three-dimensional tunnel structure, where ionic diffusion during the charge/discharge reaction is more restricted than in the two-dimensional layered structure. The lower theoretical capacity in $Li_xMn_2O_4$ is caused by the narrower reversible range (x) for Li^+ intercalation/deintercalation. The higher cell voltage may be an advantage, but in turn it is problematic because electrolytes may be decomposed during the cell cycling.[6−8] A brief review on those oxide materials leads us to conceive that the layered MnO_2 (δ-MnO_2 or naturally occurring birnessite-related MnO_2) can be an attractive candidate material because it combines in theory several advantageous features inherited from each oxide. It has a layered structure like Li_xCoO_2 and Li_xNiO_2; therefore, a high rate capability is expected. The lower cost of Mn is still a merit. In addition, its theoretical capacity is twice as large as the spinel form, given that the reversible range (x) in $Li_xMn_2O_4$ is limited to 0.0−1.0 and the same range is assumed in the layered MnO_2. Finally, the cell voltage of MnO_2 is known to be lower than the spinel $Li_xMn_2O_4$.[9] So far, there were several attempts to apply the layered MnO_2 to the cathode materials in Li secondary batteries, but the

* To whom correspondence should be addressed. Tel: +82-2-880-7074. Fax: +82-2-888-1604. E-mail: seungoh@plaza.snu.ac.kr.

† Department of Chemistry, Ewha Womans University, Seoul 120-750, Korea.

(1) Desilvestro, J.; Haas, O. *J. Electrochem. Soc.* **1990**, *137*, 5C.
(2) Ohzuku, T.; Ueda, A. *Solid State Ionics* **1994**, *69*, 201.
(3) Ohzuku, T. In *Lithium Batteries, New Materials, Developments and Perspectives*; Pistoia, G., Ed.; Elsevier: 1994; Chapter 6.
(4) Koksbang, R.; Barker, J.; Shi, H.; Saidi, M. Y. *Solid State Ionics* **1996**, *84*, 1.
(5) Nagaura, T. In *Proceedings of the 5th International Seminar on Lithium Battery Technology and Applications*; Deerfield Beach, FL, March 5−7, 1990.
(6) Jang, D. H.; Shin, Y. J.; Oh, S. M. *J. Electrochem. Soc.* **1996**, *143*, 2204.
(7) Jang, D. H.; Oh, S. M. *J. Electrochem. Soc.* **1997**, *144*, 3342.
(8) Jang, D. H.; Oh, S. M. *Electrochim. Acta* **1998**, *43*, 1023.
(9) Pistoia, G. *J. Electrochem. Soc.* **1982**, *129*, 1861.

10.1021/cm9801643 CCC: $18.00
Published on Web 02/06/1999

above-mentioned advantages are not fully realized due to the material's inferior powder characteristics as described below and/or gradual conversion to the spinel-related structure with repeated cycling.[10−12]

A variety of preparation methods for the layered MnO_2 are reported in the literature[11−24] that can be classified into two schemes: (i) the oxidation of Mn^{2+} ions by air or permanganate ions[13−17] and (ii) reduction of Mn^{7+} ions (MnO_4^- solution) with reducing agents.[11,12,17−24] Of the two, the latter method has appeared more commonly in the literature. For example, Bach et al.[19] prepared an amorphous bismuth-doped MnO_2 (birnessite) by the slow reduction of a $KMnO_4$ solution containing bismuth nitrate with concentrated nitric acid. Chen et al.[11,24] reported the formation of K_x-$MnO_2{\cdot}yH_2O$ by the hydrothermal treatment of $KMnO_4$ with nitric acid. Others proposed a sol−gel synthesis at 400−600 °C, where the gels were formed by the reduction of permanganate by fumaric acid, sugars, or other organics.[20−22] In general, these solution phase syntheses include multistep chemical reactions, and thus in order to have high purity materials, a careful control of temperature, concentration, and pH is needed in each step. Moreover, since the synthesis is carried out at lower temperature, the product powders commonly show a poor crystallinity and have a high surface area and low density. Normally, cathode materials with these characteristics are not highly sought because the materials of low-density yield batteries of low volume energy density and the materials of high surface area may provide possible reaction sites for electrolyte decomposition.[6−8] Even further, poorly crystalline materials are vulnerable to crystal stresses generated by repeated charge/discharge reactions, and thus, sometimes the structural frameworks are readily collapsed and/or they are converted to inactive phases. By contrast, high-temperature syntheses, sometimes but not always, produce powders of high crystallinity, high density, and low surface area, which are the more attractive features for battery applications.

Without a deliberate selection of synthetic conditions, however, the high-temperature preparation of layered MnO_2 is not entirely promising. As indicated in Figure 1, the layered MnO_2 compounds are known to be unstable at high temperatures.[25,26] For instance, δ-MnO_2 may be transformed to α or γ phases at 450−500 °C even under air atmosphere, and the latter phases are further reduced to the suboxides: to Mn_2O_3 at 600−800 °C and to Mn_3O_4 at >1000 °C. Even with this difficulty, it was our premise that the high-temperature preparation of layered MnO_2 could still be possible if any preparation methods satisfy at least two requisites: a high population of cations which can exert the pillaring effects to suppress the δ to γ/α transition, and a highly oxidizing atmosphere to discourage the suboxide transition. In this sense, the thermal decomposition of $KMnO_4$ is of particular interest, even if this preparation is performed at high temperatures, because the reaction medium contains both a high level of K^+ ions which may act as the pillaring cations, and the highly oxidizing species such as O_2, MnO_4^{2-}, and MnO_4^{3-}, which are produced during the pyrolyzing process.

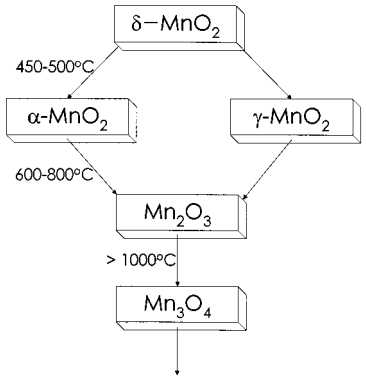

Figure 1. Thermal behavior of manganese oxides at high temperature. The nature of the stable phases and the phase transition temperature under air atmosphere are indicated.

Herbstein et al.[27] have already reported the formation of layered $K_xMnO_2{\cdot}yH_2O$ in their thermal decomposition process of $KMnO_4$. However, neither the detailed structural analysis nor the powder characteristics were provided in their report. In this work, we extended the thermal decomposition of $KMnO_4$ with several goals in mind: (i) the identification of underlying factors for the successful high-temperature preparation of layered MnO_2, (ii) the detailed structural analysis, and (iii) the improvement of both the product yield and powder characteristics. To accomplish the first goal, we examined the effects of both K/Mn ratio in the reaction medium and reaction temperature on the product quality. For the second goal, we performed the Rietveld refinement on the powder XRD pattern. For the last goal, we tried to pyrolyze the powder mixtures composed of $KMnO_4$ and manganese suboxides (MnO, Mn_3O_4, or Mn_2O_3). As a result of this work, it was found that the physicochemical properties of the product powders such as the density, surface area, and Mn^{4+} fraction are superior to those prepared by other solution-phase methods.

We also performed some preliminary experiments on the cathode properties of the layered MnO_2 in recharge-

(10) Vitins, G.; West, K. *J. Electrochem. Soc.* **1997**, *144*, 2587.
(11) Chen, R.; Whittingham, M. S. *J. Electrochem. Soc.* **1997**, *144*, L64.
(12) Le Cras, F.; Rohs, S.; Anne, M.; Strobel, P. *J. Power Sources* **1995**, *54*, 319.
(13) Yao, Y. F. U.S. Patent 4,520,005, 1985.
(14) Yao, Y. F.; Gupta, N.; Wroblowa, H. S. *J. Electroanal. Chem.* **1987**, *223*, 107.
(15) Bai, L.; Qu, D. Y.; Conway, B. E.; Zhou, Y. H.; Chowdhury, G.; Adams, W. A. *J. Electrochem. Soc.* **1993**, *140*, 884.
(16) Wadsley, A. D. *J. Am. Chem. Soc.* **1950**, *72*, 1781.
(17) Parida, K. M.; Kanungo, S. B.; Sant, B. R. *Electrochim. Acta* **1981**, *26*, 435.
(18) Cole, W. F.; Wadsley, A. D. *Trans. Electrochem. Soc.* **1947**, *92*, 133.
(19) Bach, S.; Pereira-Ramos, J.-P.; Cachet, C.; Bode, M.; Yu, L. T. *Electrochim. Acta* **1995**, *40*, 785.
(20) Bach, S.; Henry, M.; Baffier, N.; Livage, J. *J. Solid State Chem.* **1990**, *88*, 325.
(21) Le Goff, P.; Baffier, N.; Bach, S.; Pereira-Ramos, J.-P.; Messina, R. *Solid State Ionics* **1993**, *61*, 309.
(22) Ching, S.; Landrigan, J. A.; Jorgensen, M. L.; Duan, N.; Suib, S. L.; O'Young, C.-L. *Chem. Mater.* **1995**, *7*, 1604.
(23) Endo, T.; Kume, S.; Shimada, M.; Koizumi, M. *Miner. Magn.* **1974**, *39*, 559.
(24) Chen, R.; Zavalij, P.; Whittingham, M. S. *Chem. Mater.* **1996**, *8*, 1275.
(25) Moore, T. E.; Ellis, M.; Selwood, P. W. *J. Am. Chem. Soc.* **1950**, *72*, 856.
(26) Mckenzie, R. M. *Miner. Magn.* **1971**, *38*, 493.
(27) Herbstein, F. H.; Ron, G.; Weissman, A. *J. Chem. Soc. A* **1971**, 1821.

able Li cells, which is the extension of our previous report concerning the cathode properties of the layered MnO_2 in Zn/aqueous $ZnSO_4/MnO_2$ rechargeable cells.[28]

Experimental Section

Preparation and Characterizations. Before the thermal decomposition, $KMnO_4$ powder with/without manganese suboxides was ball-milled and screened through a 400 mesh sieve. The resulting powder or powder mixtures were then pyrolyzed in air for 5 h at 250−1000 °C. The heating and cooling rate was controlled at 1 °C min^{-1}. After decomposition, the soluble byproducts (K_3MnO_4 or K_2MnO_4) were removed by washing with distilled water. In this step, the washing was repeated until the initial greenish deep blue filtrate disappeared. The resulting powders were dried under vacuum and stored under ambient condition.

The crystal structure of the resulting powders was identified by XRD (X-ray diffraction) analysis, and one of them (the 800 °C data) was refined by the Rietveld method.[29] The ultimate goal of the refinement was, instead of having lower R values, to find the proper space group with which all the observed diffraction peaks can be assigned.. In this sense, the lower angle data ($2\theta < 30°$) were excluded because only the (002) and (004) peaks appeared in this range and the intensity of these is rather significantly influenced by the preferred orientation effect.[30,40] Also, those lower angle peaks were so much stronger than the higher angle ones that they were weighted too heavily in the refinement process, leading to a wrong assignment with some peaks being left unindexed. Reflection positions and intensities were calculated for both Cu $K\alpha_1$ and $K\alpha_2$ reflections. At the initial stage, we tried to find the best-fitted structural model by comparing the diffraction data with the predefined birnessite structural model, such as monoclinic,[30−33] orthorhombic,[33,34] tetragonal,[27] and hexagonal[24,31−33,35−37] ones. Among those, the hexagonal system provided the best fit with a minimal number of unindexed peaks. Next, the scale factor, background and profile-shape coefficients, unit-cell parameters, and zero point (in 2θ) correction factors were refined. The background was calculated using a sixth-order polynomial, and the observed peak shapes were approximated with a pseudo-Voigt profile function. Even though an attempt to locate the nonunique atomic positions might lead to a better refinement, these factors were ignored in order to obtain an approximate and simple structural model (space group, unit cell, and layered structural model), since our concern was largely limited to find the relationship between the layered structural model (viz., P2, P3, O2, O3, O6 class)[38] and the electrochemical characteristics.[39] Only the overall temperature factor was refined.[24,40] After the preliminary step, the refinement was further continued until the R_p (pattern R-factor) and R_{wp} (weighted pattern R-factor) were minimized.

Surface area was measured by the Brunauer−Emmett−Teller (BET) method and the powder morphology was examined by scanning electron microscopy (SEM). The K^+ ion contents were analyzed by an inductively coupled plasma (ICP) technique. The total Mn contents and average Mn valence were analyzed by the potentiometric titration method.[41]

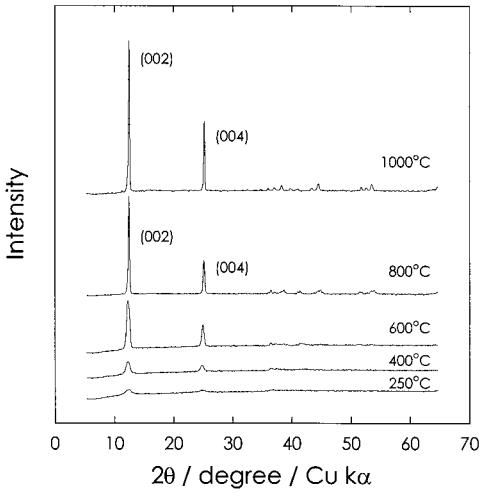

Figure 2. XRD powder patterns of the layered MnO_2 prepared at 250−1000 °C. Note that the (002) and (004) diffraction lines are dominant in each profile.

Cathodic Performances of Layered MnO_2. To prepare the cathodes, a pasted mixture of MnO_2 powder, carbon additive, and poly(tetrafluoroethylene) (PTFE) binder was pressed onto a stainless steel exmet (apparent area = 1 cm^2) and dried under vacuum. Li foil (area = ca. 1.5 cm^2) was used as the anode and reference electrode. The used electrolyte was PC + DME (1:1 vol ratio)/1 M $LiClO_4$, where PC is propylene carbonate and DME is dimethoxyethane. In order for the cell capacity to be limited by the cathode such that the observed capacity represents those of the cathodes, an excess amount of Li metal was used as the anode. The galvanostatic charge/discharge behavior was analyzed within a voltage cutoff range of 2.0−4.3V (vs Li/Li^+). The electrochemical voltage spectroscopy (EVS) was utilized to examine the cell reactions occurring at the cathode materials. For this measurement, an EG&G PARC M362 potentiostat and a programmable voltage source were combined to control the applied voltage step, and the current was continuously monitored until it decayed to a preset threshold value ($I_{threshold}$). The cell potential was increased in stepwise by dV (=0.01 V). All the experiments were carried out at 25 ± 1 °C in an Ar-filled drybox.

Results and Discussion

Preparation and Structural Analysis of Layered MnO_2. Typical XRD powder patterns of the layered MnO_2 products are reproduced in Figure 2. Regardless of the preparation temperature, the powders show only diffraction lines of layered MnO_2 phase without impurity lines of cryptomelane (α-MnO_2), ramsdellite (γ-MnO_2), or manganese suboxides. It is apparent in Figure 2 that the lower angle (00l) peaks are much stronger than the others, which may arise from a preferred orientation.[32] Figure 3 shows the SEM photographs of the 400 °C- and 800 °C-prepared powders, where the presence of lamella-type crystallites is readily recognized, particularly in the 800 °C-prepared powder. If the powder is spherically shaped or finely grained, there may be a less preferred orientation effect. However, the present sample is unground and of conspicuous

(28) Kim, S. H.; Oh, S. M. *J. Power Sources* **1998**, *72*, 150.
(29) Sakthivel, A.; Young, R. A. In *User's Guide to Programs DBWS-9006 and DBWS-9006PC*; Georgia Institute of Technology, **1990**.
(30) Post, J. E.; Veblen, D. R. *Am. Mineral.* **1990**, *75*, 477.
(31) Le Goff, P.; Baffier, N.; Bach, S.; Pereira-Ramos, J.-P.; Messina, R. *J. Mater. Chem.* **1994**, *4*, 133.
(32) Le Goff, P.; Baffier, N.; Bach, S.; Pereira-Ramos, J.-P.; Messina, R. *J. Mater. Chem.* **1994**, *4*, 875.
(33) Parant, J.-P.; Olazcuaga, R.; Devalette, M.; Fouassier, C.; Hagenmuller, P. *J. Solid State Chem.* **1971**, *3*, 1.
(34) JCPDS 23-1046.
(35) Strobel, P.; Charenton, J. C. *Rev. Chim. Miner.* **1987**, *24*, 199.
(36) Strobel, P.; Mouget, C. *Mater. Res. Bull.* **1993**, *28*, 93.
(37) JCPDS 23-1239.
(38) Delmas, C. In *Lithium Batteries, New Materials, Developments and Perspectives*, Pistoia, G., Ed.; Elsevier: New York, 1994; Chapter 12.
(39) Manuscript in preparation.
(40) Post, J. E.; Bish, D. L. *Am. Mineral.* **1988**, *73*, 861.
(41) Jeffery, G. H.; Bassett, J.; Mendham, J.; Denney, R. C. In *Vogel's Textbook of Quantitative Chemical Analysis*, 5th ed.; Longman: Harlow, U.K., 1989; p 584.
(42) Baker, J. *Electrochim. Acta* **1995**, *40*, 1603.
(43) Baker, J.; Koksbang, R. *Solid State Ionics* **1995**, *78*, 161.

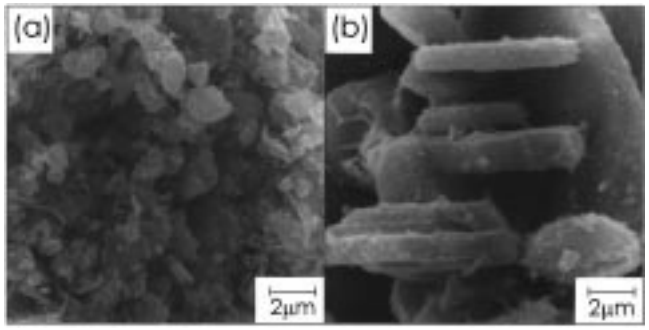

Figure 3. SEM photographs showing the crystal shape of MnO_2 pyrolyzed at (a) 400 °C and (b) 800 °C. Note the well-grown lamella-type crystallites in the 800 °C-prepared sample.

platelike shape. Therefore, the XRD data are very likely influenced by the preferred orientation effects.

There is a considerable discrepancy as to the structure of layered MnO_2 in the literature. Delmas et al. reported that there are two forms of layered MnO_2 that differ in the Mn/O ratio.[44] The more oxygen-rich phase that is stable at lower temperatures, viz., $K_{0.47}Mn_{0.94}O_2$, has a hexagonal structure, whereas the higher temperature stable phases have a monoclinically distorted structure. Naturally occurring layered MnO_2, called birnessite, has recently been reported to be simple hexagonal,[31−33,35−37] while the synthetic compounds are monoclinic,[30−33] orthorhombic,[33,34] tetragonal,[27] or rhombohedral.[24] The discrepancy in the structural analysis likely comes from, among others, the material's uncertainties, such as the low crystallinity, contamination with impurities, and structural disorders. In this study, precise structural analysis was even more difficult due to the low intensity at the higher angle diffraction lines. Only the powder prepared at >800 °C provided reasonably intense diffraction lines at higher angles, such that we collected the diffraction data of the 800 °C-prepared sample at $2\theta = 30-70°$ with a slow scan rate for Rietveld refinement. After a careful examination of the powder pattern, a hexagonal unit cell (space group = $P6_3/mmc$), rather than the monoclinic or orthorhombic ones, could be chosen as a starting model, with which all the diffraction peaks except four could be indexed and fitted with reasonably small *R*-factors. The resulting crystallographic parameters of $K_{0.30}MnO_{2.11}\cdot 0.6H_2O$ (800 °C) are listed in Table 1.

The observed and calculated diffraction profiles are presented in Figure 4 and the 14 observed diffractions with the indices, angles in degree (2θ), and *d* spacings are listed in Table 2. Also, the calculated 14 Bragg reflection positions are marked in Figure 4 as vertical bars. As shown in Figure 4, the observed and calculated diffraction profiles are well-matched to each other, except for the peaks appearing at ca. 40°, 44°, 53°, and 63° 2θ. These unindexed peaks are likely the trace of a superstructure (orthorhombic, $a_{ort} = \sqrt{3}a_{hex}$, $b_{ort} = b_{hex}$, $c_{ort} = c_{hex}$) which arises from a slight lattice distortion within the layers, probably due to defects in the Mn or O sites. Actually, the diffraction angle of these unindexed peaks was matched with that observed with a layered MnO_2 having an orthorhombic lattice (space group = *Cmcm*, $a = 4.95$ Å, $b = 2.98$ Å, and $c = 14.2$ Å).[39] Also, owing to the preferred orientation, the (006), (008), and (0010) peaks in the observed pattern are slightly stronger than calculated.

(44) Delmas, C.; Fouassier, C. *Z. Anorg. Allg. Chem.* **1976**, *420*, 184.

Table 1. Refined Crystallographic Parameters for $K_{0.30}MnO_{2.11}\cdot 0.60H_2O$ (preparation temp = 800 °C)

atom	site	*x*	*y*	*z*	occupancy (%)	thermal[a] (Å^2)
Mn	2a	0	0	0	95(2)	0.11(1)
O	4f	$^1/_3$	$^2/_3$	0.0693(2)[b]	100	0.11(1)
K	2d	$^2/_3$	$^1/_3$	$^1/_4$	29(2)	0.11(1)

crystal symmetry	hexagonal	radiation	Cu Kα
space group	$P6_3/mmc$ (No. 194)	R_p[d]	1.05(1) %
cell parameter		R_{wp}[d]	1.47(1) %
a	2.842(1) Å	$R_{expected}$[d]	3.74(1)%
c[c]	14.16(1) Å	R_{Bragg}[d]	13.2(1)%

[a] Overall isotropic temperature factors were used. [b] Standard deviations. [c] The repeat distance (*c*/2) was found to vary from sample to sample between 6.98 and 7.35 Å, due to the variations in the relative humidity and interlayer water content. [d] *R*-factors: $R_p = 100\Sigma|y_i - y_{ci}|/\Sigma|y_i|$, pattern *R*-factor; $R_{wp} = 100(\Sigma w_i(y_i - y_{ci})^2/\Sigma w_i y_i^2)^{1/2}$, weighted pattern *R*-factor; $R_{expected} = 100((N - P + C)/\Sigma w_i y_i^2)^{1/2}$, expected R-factor; $R_{Bragg} = 100\Sigma|I_o - I_c|/\Sigma|I_o|$, Bragg *R*-factor. y_i, y_{ci}, and w_i are the observed, calculated intensity, and weighted factor at each sampling steps, respectively; *N*, *P*, and *C* are the numbers of observation, refined parameters, and constraints, respectively; and I_o and I_c are the observed and calculated intensity at each Bragg reflection position.

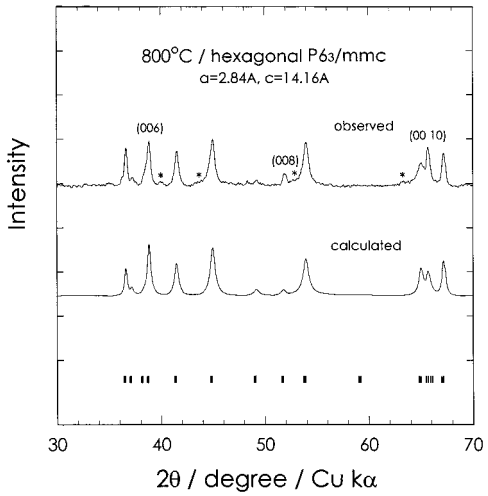

Figure 4. Result of Rietveld refinement on the layered MnO_2 prepared at 800 °C. Note that the observed (006), (008), and (0010) peaks are slightly stronger than those calculated and there are some unindexed peaks marked as (∗). Crystallographic parameters and XRD data are listed in Tables 1 and 2, respectively.

Figure 5 shows a schematic drawing of the hexagonal lattice. This structure can be described as a P2-type structure, where the manganese ions in the layer plane [two Mn in the 2a (0 0 0) site] are octahedrally coordinated and the oxide ions in the layer plane [four O in the 4f ($^1/_3$ $^2/_3$ 0.0693) site) provide trigonal prismatic sites [2d ($^2/_3$ $^1/_3$ $^1/_4$) site] for the K^+ ions and H_2O in the interlayer gap. Thus, the stacking pattern parallel to the *z* axis can be described as AaBb′BcAd′ (P2-type), where A and B represent the position of oxide ions, a and c the position of the manganese ions, and b′ and d′ the position of K^+ ions and H_2O (Figure 5b). The P2-type structure is not common in layered oxides, whereas the O3-type with three layers in the unit cell and pillaring cations at the octahedral sites is more often found in layered materials.[38] The repeat distance 7.08

Table 2. XRD Data for $K_{0.30}MnO_{2.11}\cdot 0.60H_2O$ (preparation temp = 800 °C)

h	*k*	*l*	position (θ)	d-spacing (Å)
0	0	2	12.50	7.078
0	0	4	25.15	3.539
0	1	0	36.43	2.464
0	1	1	37.00	2.428
0	0	6	38.11	2.359
0	1	2	38.66	2.327
0	1	3	41.30	2.184
0	1	4	44.78	2.022
0	1	5	48.97	1.859
0	0	8	51.61	1.769
0	1	6	53.75	1.704
0	1	7	59.05	1.563
0	1	8	64.82	1.437
1	1	0	65.51	1.424
0	0	10	65.94	1.416
1	1	2	67.00	1.396

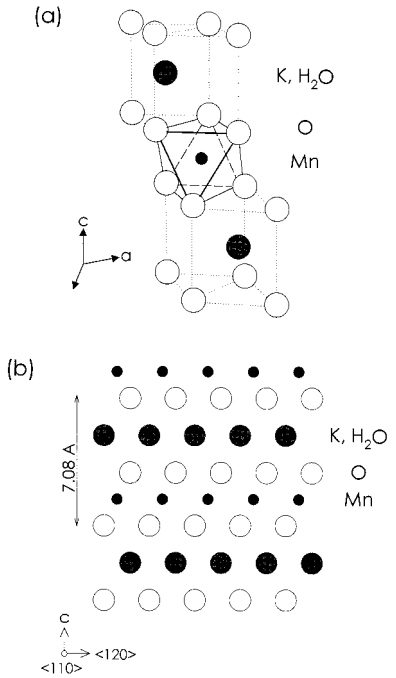

Figure 5. Schematic illustration of the structure of layered MnO_2 prepared at 800 °C: (a) three-dimensional view showing that Mn ions are located in octahedral sites and K^+ and H_2O in trigonal prismatic sites and (b) ⟨110⟩ projection indicating the P2-type stacking pattern.

Å is comparable to that observed with potassium or sodium birnessite, where K^+ or Na^+ ions and water molecules share the interlayer space.[21,22]

Table 3 summarizes the surface area, chemical composition, powder tap density,[45] and product yield of the resulting powders as a function of preparation temperature and starting powder mixtures. The list is divided into two groups: the first series (sample **1**−**5**) was prepared from pure $KMnO_4$ powder, whereas the second series (sample **6**−**8**) was prepared from the mixture of $KMnO_4$ and manganese suboxides. In the first series, the surface area shows a tendency to decrease from 18 to 2 $m^2\ g^{-1}$ with an increasing preparation temperature at 250−1000 °C. The powder density steadily increases with temperature to reach 1.36 g cm^{-3} at 1000 °C. These observed tap densities are substantially higher than those of low-temperature solution-phase synthesized MnO_2 powders (ca. 0.7 g cm^{-3}).[13,46] The total Mn content and Mn^{4+} fraction in the product powders are also listed in Table 3 and graphically presented in Figure 6. As the pyrolyzing temperature increases, the total Mn content increases, whereas the Mn^{4+} fraction shows the opposite trend. When $KMnO_4$ is pyrolyzed at >800 °C, the total Mn fraction is >50% over the total mass, about 85−92% being Mn^{4+} ions. Given that the layered MnO_2 transforms to other suboxides when it is heat-treated at >600 °C in air, the observed high population of Mn^{4+} ions in the samples supports the premise that the pyrolyzing media provide a highly oxidative atmosphere so as to discourage the suboxide transition. The manganese dioxides prepared in this work show a wide range of oxygen stoichiometry depending on the preparation condition. A brief look at the formula units for samples **1**−**5** reveals that the oxygen stoichiometry steadily decreases with temperature. This is not surprising because oxygen-deficient manganese oxides become favored at higher temperatures, as mentioned in the introduction.

The chemical formula listed in Table 3 illustrates that the present products contain much lower K^+ ions as compared to the Herbstein's product, $K_{0.57}MnO_{2.29}\cdot 0.71H_2O$. This difference seems to arise from the different washing method: Herbstein et al. washed the products with a KOH solution, whereas we washed with distilled water. It is thus likely that, in the Herbstein's powders, extra K^+ ions were incorporated during the washing period.

Table 3 also illustrates that the alkali metal/Mn ratio and average Mn valence are somewhat different than those prepared by the sol−gel methods. For example, Bach et al.[21] prepared a sodium birnessite formulated as $Na_{0.45}MnO_{2.14}\cdot 0.76H_2O$, where the alkali metal content is rather higher than our samples. The lower K^+ incorporation in the present samples in turn reflects the higher Mn valence, since the oxygen stoichiometry factors are comparable between the two samples. Given that the chemical composition of another sol−gel derived material by Ching et al[22] is $K_{0.28}MnO_{1.98}\cdot 0.19H_2O$, the present products, for instance the 800 °C-prepared powder, contain a similar amount of K^+ ions but a higher oxygen content, thereby giving a higher Mn valence. In short, the layered MnO_2 prepared herein have higher Mn valence as compared to those prepared by other methods, which is an important advantage with regard to the theoretical capacity. The theoretical capacity of the present samples is calculated to be 210−230 mA h g^{-1} assuming a one-electron charge/discharge reaction, which is higher than that of spinel $Li_xMn_2O_4$ (148 mA h g^{-1}).

Improvement of Product Yield. As listed in Table 3, the pyrolysis of $KMnO_4$ gives a product yield 67−79% based on the Mn molar quantity. The other portion of Mn is converted to the water-soluble byproducts (K_2MnO_4 or K_3MnO_4) and removed during the washing period. To reduce this waste, thermal decomposition was performed with the mixtures of $KMnO_4$ and manganese suboxides (Mn_2O_3, Mn_3O_4, or MnO). The XRD patterns traced with the resulting products are reproduced in Figure 7, where the used suboxide and K/Mn atomic

(45) *ASTM* No. B527-93.

(46) Kainthia, R. C.; Manko, D. J. U.S. Patent 5,156,934, 1992.

Table 3. Physicochemical Properties of Layered MnO_2 Powders Prepared at Different Temperature and with Different Starting Materials

no.	temp (°C)	source	surface area (m^2/g)	total Mn content (wt%)	Mn^{4+} (%)	K^+ (wt%)	formula	powder density[b] (g/mL)	yield (Mn%)
1	250	$KMnO_4$	18.4	48.8	96.4	9.3	$K_{0.27}MnO_{2.12}0.89H_2O$	0.56	66.6
2	400	$KMnO_4$	16.6	48.5	94.5	10.7	$K_{0.31}MnO_{2.13}0.76H_2O$	0.58	72.3
3	600	$KMnO_4$	10.0	49.2	93.9	10.4	$K_{0.30}MnO_{2.12}0.61H_2O$	0.75	73.1
4	800	$KMnO_4$	4.9	49.2	92.0	10.4	$K_{0.30}MnO_{2.11}0.60H_2O$	1.10	73.3
5	1000	$KMnO_4$	2.3	50.1	85.3	10.6	$K_{0.30}MnO_{2.07}0.47H_2O$	1.36	78.6
6[a]	800	$KMnO_4 + Mn_2O_3$	4.0	52.3	71.7	10.5	$K_{0.28}MnO_{2.00}0.56H_2O$	1.15	96.4
7[a]	800	$KMnO_4 + Mn_3O_4$	6.5	52.8	67.8	10.8	$K_{0.29}MnO_{1.98}0.56H_2O$	1.33	98.0
8[a]	800	$KMnO_4$ + MnO	8.0	54.1	62.5	9.5	$K_{0.25}MnO_{1.94}0.54H_2O$	1.52	98.0

[a] The molar ratio of $KMnO_4$/suboxide was adjusted to meet the condition of K/Mn atomic ratio = 0.5. [b] Powder tap density was measured according to the ASTM standards no. B 527-93.

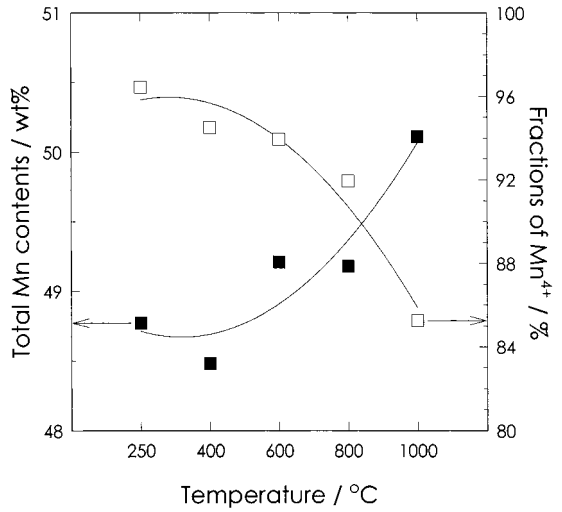

Figure 6. Total Mn content (wt %) in the samples and Mn^{4+} fractions (%) as a function of the preparation temperature.

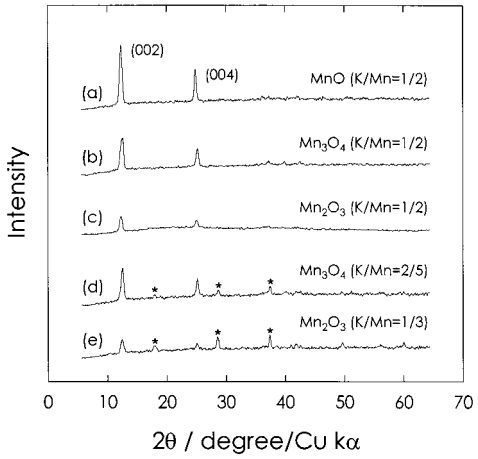

Figure 7. XRD patterns of the layered MnO_2 powders prepared from the mixture of $KMnO_4$ and manganese suboxides (800 °C). The used manganese suboxides and K/Mn atomic ratio in the reactants are indicated. The diffraction lines assigned to α-MnO_2 phase are marked as (*).

ratio are indicated. An inspection of the powder patterns reveals that in some trials only the peaks of layered MnO_2 appear, whereas in others the diffraction lines belonging to α-MnO_2 are also detected. The key determinant for the purity of layered MnO_2 turns out to be the K/Mn atomic ratio in the reactant mixtures. For instance, when the K/Mn ratio is <0.5, the products are always contaminated with α-MnO_2 regardless of the suboxides used (Figure 7d,e). Interestingly, however, if the ratio is >0.5, the layered MnO_2 is the only detectable product irrespective of the used suboxides. The secret for the successful syntheses cannot be fully explained, but given the fact that K^+ content in the interlayer gap is directly related to the thermal stability of layered framework, one may infer that if the K/Mn ratio is low, some portion of the layered phase is converted to α-MnO_2 due to the shortage of K^+ ions in the pyrolyzing media. A similarity can be found in Na_xMnO_2 compounds, where if the Na^+ content is lower than a certain level (x < 0.7), the three-dimensional structure is more dominant than the layered one.[33]

The powder properties of the second series products (sample **6**−**8**) are listed in Table 3. As shown, they are quite similar to those of the first series except that the product yields reach up to 98%, but the Mn^{4+} fractions are somewhat lower in the second series. This lower Mn^{4+} fraction in turn indicates the lower oxygen stoichiometry in the latter products. From the observation that the oxygen stoichiometry, δ in $K_xMnO_{2+\delta}{\cdot}yH_2O$, becomes smaller as the more oxygen-deficient suboxides are used as the reagent (see the formula units of sample **6**−**8**), the lower δ can readily be ascribed to the low oxygen contents in the reaction media.

Cathode Performances of Layered MnO_2 in Li Secondary Batteries. Figure 8a shows the cycling behavior of the 800 °C-prepared MnO_2 powder in Li/PC + DME−$LiClO_4$/MnO_2 cells. The initial discharge capacity was 175 mA h g^{-1}, which amounts to 75% of the theoretical value based on a one-electron reaction, and more than 75% of the initial value was retained after 50 cycles.

A typical galvanostatic charge/discharge profile is reproduced in Figure 8b, where the lower profile corresponds to the discharging curve and the upper one the charging curve. The layered MnO_2 in this system discharges in one step (one-electron reaction), and also the charging profile shows a one-step reaction. This can be more apparent in the EVS profile shown in Figure 8c, where the discharging reaction takes place at 2.7−3.0 V and the charging reaction mainly at 3.0−3.2 V. The electrochemical reactions taking place at the end of charging period (>3.7 V) are seemingly related with the electrolyte decomposition.[6−8] The EVS profile did not change along with cell cycling; in particular, no peaks related with the spinel phases appeared near 4.0 V. As mentioned earlier, several previous reports complained that layered MnO_2 cathodes degrade to the spinel-related structures with cell cycling.[10−12] The absence of spinel transition in these materials seems

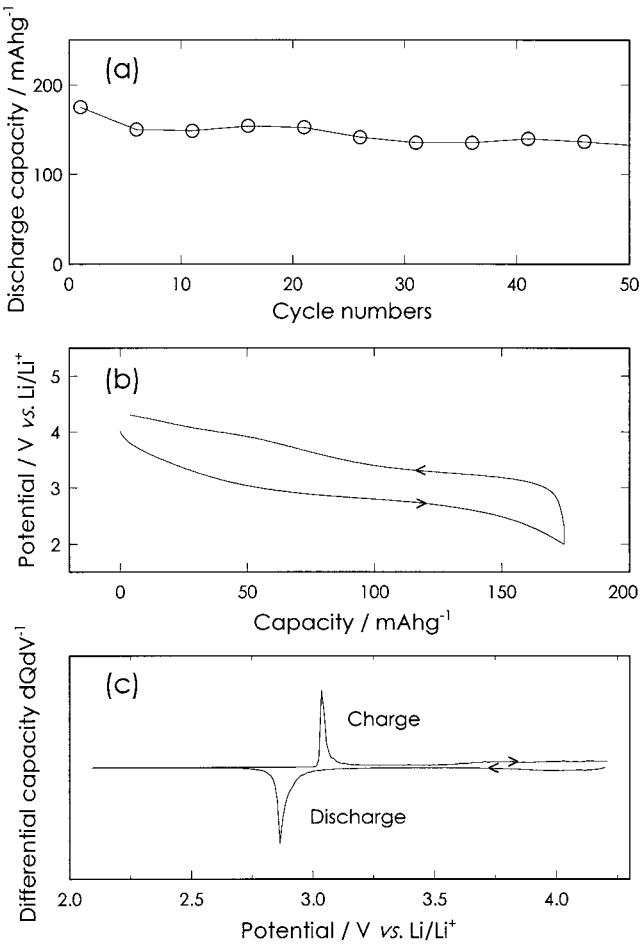

Figure 8. Cell performances observed with an Li/PC + DME−$LiClO_4$/MnO_2 cell: (a) the discharge capacity against the cycle numbers, (b) the charge/discharge potential profile traced in the first cycle, and (c) the EVS profile recorded with the cathode. The cathode was composed of MnO_2 powder (800 °C), Ketjen Black, and PTFE (15:2:1 wt ratio). The galvanostatic charge/discharge cycling was performed at 1 mA cm^{-2} (0.4 C rate) in the potential range of 2.0−4.3 V (vs Li/Li$^+$).

to stem from the difference in the oxide packing patterns,[47] i.e., the P2-type structure in the present samples but the O3-type in spinels. Details on the cathode performances will be reported in the forthcoming paper.[39]

Conclusions

In this work, we prepared the layered MnO_2 by thermally decomposing $KMnO_4$ or a mixture of $KMnO_4$ and manganese suboxides. Particular goals were to prepare powder products suitable for battery applications, to identify the underlying parameters for the formation of a layered structure, and to characterize the crystal structure of the resulting materials. In addition, we tested their applicability to Li secondary cells. The following points would be of value.

(i) Although layered MnO_2 is thermally unstable at high temperatures, the present method produces a highly crystalline layered MnO_2 without noticeable impurities such as α- or γ-MnO_2 phases and suboxides. It is likely that a high population of K^+ ions present in the reaction media act as pillaring cations to stabilize the layered framework and the highly oxidizing species produced during the thermal decomposition suppress the suboxide transition. The importance of K^+ ions for the formation of a layered structure is also found in the mixture decomposition, where it was found that if the K^+ content is higher than a certain level (K/Mn > 0.5), only the layered phase forms regardless of the suboxides used.

(ii) The 800 °C-prepared material has a formula unit $K_{0.30}MnO_{2.11}\cdot 0.60H_2O$, where K^+ ions and water molecules locate at the interlayer gap. The best Rietveld refinement on this material was achieved with a hexagonal unit cell and $P6_3/mmc$ space group. The resulting cell parameters were $a = 2.84$ Å and $c = 14.16$ Å.

(iii) The resulting layered MnO_2 powders carry some of the desirable characteristics for battery applications, such as the high powder density and high Mn^{4+} fraction. The theoretical capacity was 210−230 mA h g^{-1} based on a one-electron charge/discharge reaction, which is higher than the spinel $Li_xMn_2O_4$. Also, a product yield up to 98% was achieved by the decomposition of the mixture.

(iv) In the Li rechargeable cells, the materials show some promising features, such as high capacity and good cyclability without spinel transition.

Acknowledgment. This study was supported by Korean Ministry of Education through Research Fund. Also, S.-J.K. thanks KOSEF (K-N96048) for financial support.

CM9801643

(47) Kim, S. H.; Oh, S. M. In *Proceedings of the 9th International Meeting on Lithium Batteries*; Edinburgh, 1998.